Watching a Full Photocatalytic Cycle by Electron Paramagnetic Resonance

Jian-Qing Qi[1]†, Weiqun Suo[1]†, Jing Liu[1], Songtao Sun[1], Lei Jiao[1*], Xingwei Guo[1*]

[1] Center of Basic Molecular Science (CBMS), Department of Chemistry, Tsinghua University; Beijing 100084, China.
† These authors contributed equally to this work.

*Corresponding author. Email: leijiao@mail.tsinghua.edu.cn; xingwei_guo@mail.tsinghua.edu.cn.

Abstract: Molecular photocatalysis has shown tremendous success in sustainable energy and chemical synthesis. However, visualizing the intricate mechanisms in photocatalysis is a significant and long-standing challenge. By employing our recently developed sensitivity-enhanced time-resolved electron paramagnetic resonance technique, we directly observed all radicals and radical ions involved in the photocatalytic addition of a tertiary amine to *tert*-butyl acrylate. The full picture of the photocatalytic cycle has been vividly illustrated by the fine structures, chemical kinetics, and dynamic spin polarization of all open-shell intermediates directly observed in this prototypical system. Given the universality of this methodology, we believe it greatly empowers the research paradigm of direct observation in both photocatalysis and radical chemistry.

Introduction

Photocatalytic reactions harness the energy of light to facilitate chemical transformations, enabling various applications such as water splitting, carbon dioxide reduction, pollutant degradation, and organic synthesis (*1,2,3,4,5,6,7,8*). A crucial aspect of advancing photocatalysis is understanding their mechanisms (*9,10*). In the realm of molecular photocatalysis, the catalytic cycles generally involve several reactive and short-lived radical intermediates, presenting a formidable challenge for mechanistic studies. Most mechanistic studies have to rely on indirect methods such as product analysis, apparent kinetics, and spin trapping (*11*). The ability to directly "watch" the evolution of radical intermediates in a photocatalytic reaction has long been a coveted goal for many chemists.

Over the past decades, transient absorption (TA) and time-resolved electron paramagnetic resonance (TREPR) spectroscopy have been used in the study of transient radical species (*12,13,14,15,16,17,18,19,20,21,22*), which offered valuable mechanistic insights into a number of elementary radical reactions. However, these existing techniques have limitations when it comes to studying the whole cycle of a photocatalytic reaction. Electronic or vibrational TA spectroscopy lacks specificity for radicals, hampering the identification of different radical intermediates in the cycle. On the other hand, the current TREPR technique suffers from inherent low sensitivity and limited observation time window depends on the time-domain of hyperpolarization (*17,23*), making it incapable of observing the complete progression of multi-step reaction cascades. As a result, direct observation of a photocatalytic cycle with precise characterization and tracking of each radical intermediate remains unprecedented using existing techniques. This highlights the pressing need for an advanced time-resolved spectroscopic method that provides both fine structural information and exceptional sensitivity.

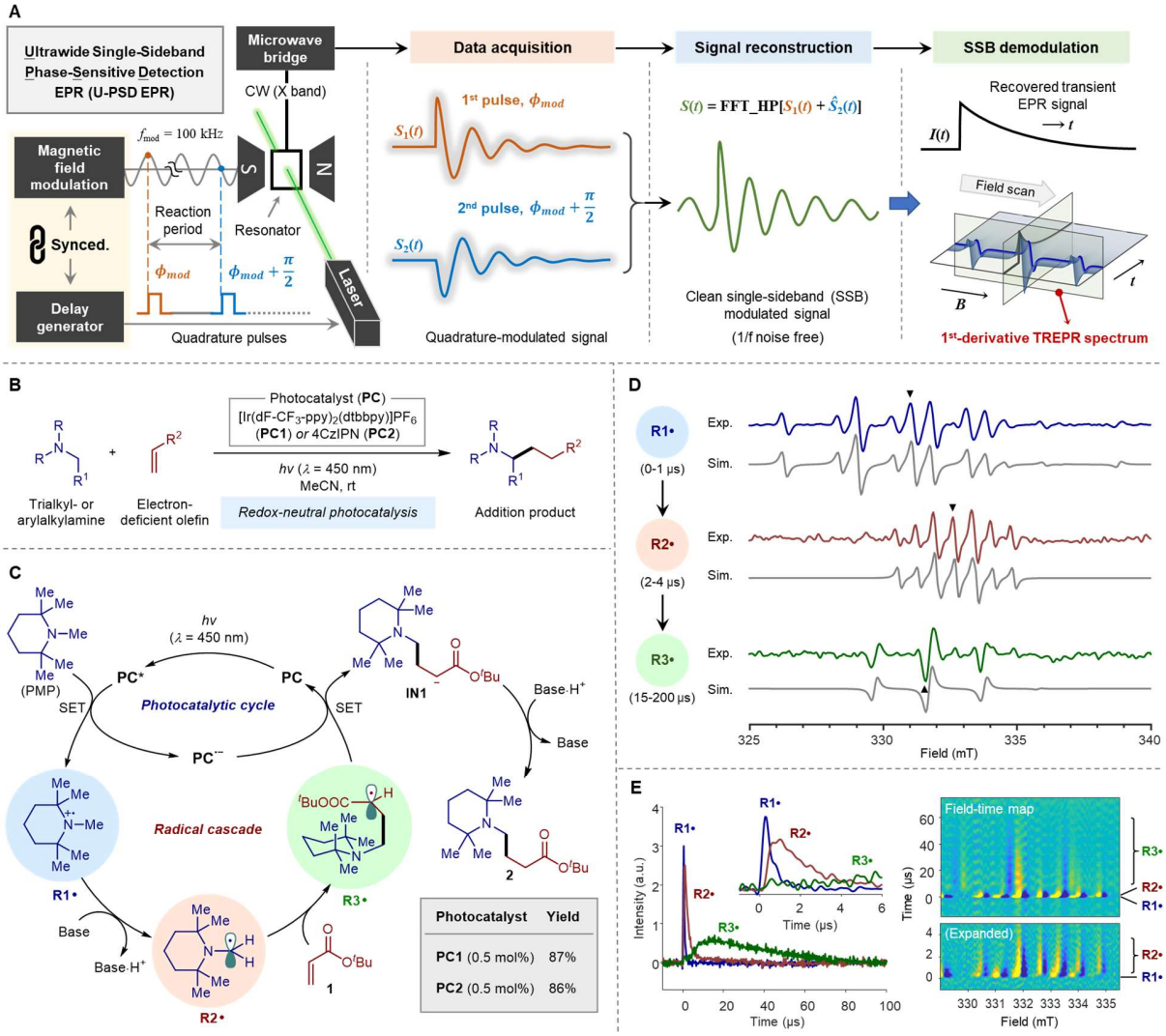

Fig. 1. Watching a photocatalytic radical cascade using the U-PSD EPR technique. (**A**) Schematic interpretation of the U-PSD EPR technique. (**B**) General reaction scheme of the photocatalyzed addition of amines to olefins. (**C**) Proposed mechanism of the reaction between pempidine and *tert*-butyl acrylate. (**D**) Time-resolved EPR spectra of the three radical intermediates (X-band, 9.33 GHz). The peaks marked with a black triangle were used to acquire the kinetic profiles of the corresponding radicals. (**E**) Kinetic traces of the radicals involved and the field-time map of the reaction. Exp., experimental; Sim., simulated.

We have recently invented a new EPR technique which we named the ultrawide single sideband phase-sensitive detection (U-PSD) TREPR (Fig. 1A) (*24*). Unlike the traditional continuous wave (CW) direct detection TREPR, this technique utilizes precisely controlled sequence of laser pulses and magnetic field modulation to generate a pair of quadrature-modulated EPR signals. These signals are used by an innovative algorithm to reconstruct a clean single-sideband (SSB) modulated signal, effectively suppressing 1/*f* noise. By employing SSB demodulation, we could accurately retrieve the transient EPR signal, resulting in first-derivative EPR spectra with both high time-resolution and exceptional sensitivity. This advancement enables the detection of weak signals of transient radicals in a solution-phase chemical reaction over a wide time range, which was previously not possible with existing TREPR techniques. Herein, we present the first direct observation of all open-shell intermediates in a full photocatalytic cycle using this technique,

which provides mechanistic insights into the photocatalytic radical reaction with an unprecedented level of detail.

Results and Discussion

We focused on a representative photocatalytic reaction, the addition of amine α-C-H bonds to alkenes promoted by visible light (*25*), which can be catalyzed by several photoredox catalysts (Fig. 1B). As a model, the reaction of pempidine (*N*,2,2,6,6-pentamethylpiperidine, PMP) with *tert*-butyl acrylate (**1**) under visible light (450 nm) catalyzed by either an iridium-based photocatalyst [Ir(dF-CF_3-ppy)$_2$(dtbbpy)]PF_6 (**PC1**) or an organic photocatalyst 4CzIPN (**PC2**) afforded Giese-type adduct **2** in good yields (Table S1). This reaction is believed to proceed through a typical redox-neutral photocatalytic cycle involving elementary steps of single electron oxidation, proton transfer, radical addition, and single electron reduction (*25*), with the formation of three key radical intermediates **R1•** to **R3•** (Fig. 1C). Although this catalytic cycle is commonly proposed previously, it has never been directly observed experimentally.

Holistic observation of the radical cascade

The U-PSD EPR technique has transformed the proposed reaction mechanism into observed reality. The measurements were done by flowing an acetonitrile solution of PMP, **1**, the photocatalyst, and 4-dimethylaminopyridine (DMAP) through the resonator of the spectrometer while applying repeated laser pulses at 298 K. In the reaction catalyzed by **PC1**, three radical species were identified in different time regions. These species have been unambiguously identified as the amine radical cation (**R1•**), α-aminoalkyl radical (**R2•**), and the radical adduct (**R3•**), which was achieved by analyzing the structural information (Figs. S2-4), specifically the hyperfine splittings (HFSs), extracted from the well-resolved TREPR spectra (Fig. 1D). It is notable that the acquired TREPR spectra exhibited a hyperpolarized pattern, providing key information for the SET steps (*vide infra*).

The kinetic profiles of these species were determined by monitoring the non-overlapping EPR peaks (Fig. 1E, left). The kinetic plots indicated the sequential formation of **R1•**, **R2•**, and **R3•**, with distinct lifetimes in the reaction system. This aligns well with the proposed reaction pathway of **R1•** → **R2•** → **R3•**. The observed kinetic traces provide valuable information about the lifetime of these radicals as well as their spin dynamics (Fig. S5). A field-time map constructed using the acquired TREPR data exhibited the panorama of the evolution of radical intermediates over the reaction time course (Fig. 1E, right, see Fig S6 for details).

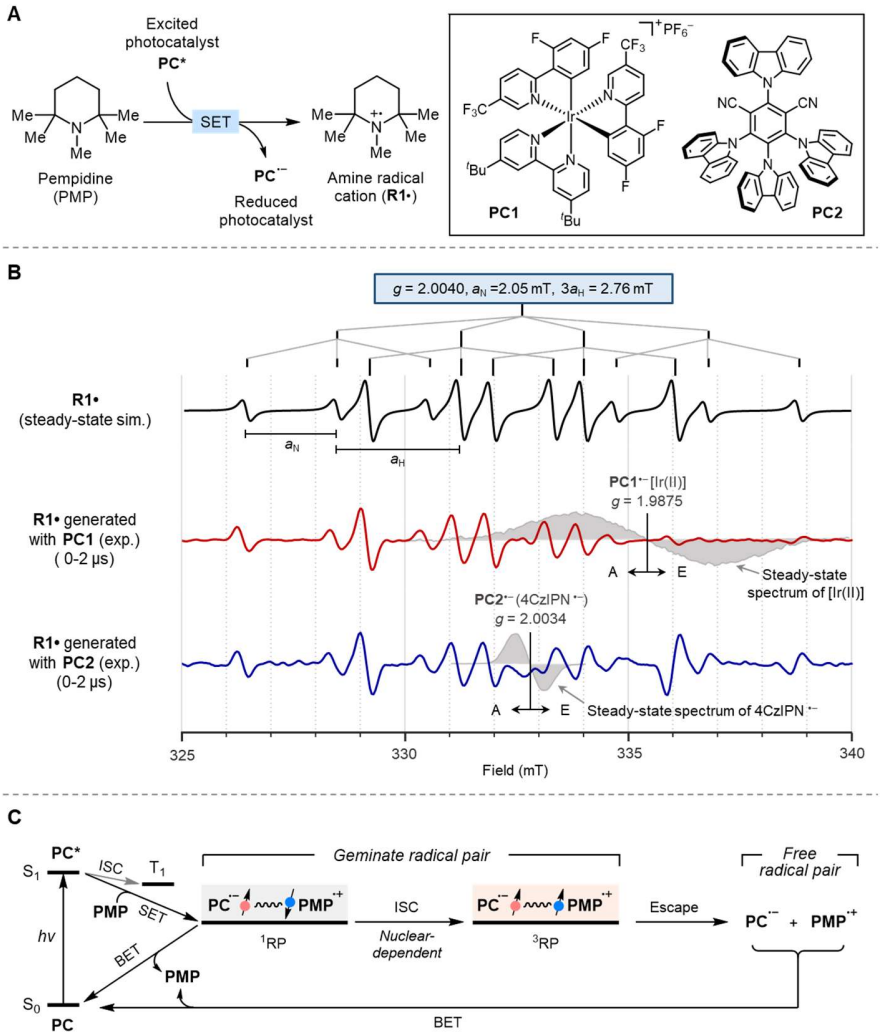

Fig. 2. Observing the SET oxidation of pempidine by the excited photocatalyst. (**A**) The photoinduced SET reaction. (**B**) EPR spectra of **R1•** under Boltzmann distributed spin state (simulated, black) and generated with **PC1** (red) and **PC2** (blue). (**C**) The geminate radical pair mechanism of the photoinduced SET. ISC, Internal system crossing; BET, back electron transfer; RP, radical pair.

Photoinduced single-electron oxidation of the amine substrate

In addition to identifying and tracing of all radical intermediates, we were able to acquire more detailed information about each individual step. We then focused on the initial SET step of the radical cascade resulting in the formation of the amine cation radical **R1•** through the photoinduced SET between PMP and **PC1** or **PC2** (Fig. 2A). The measurements were done using simplified reaction system only consisting of PMP and the photocatalyst. The TREPR spectra acquired by integrating 0-2 µs after the laser pulse (Fig. 2B, red and blue spectra) confirmed the formation of the same radical intermediate with different photocatalysts, as identical splitting pattern were observed. The simulated steady-state EPR spectrum of **R1•** (Fig. 2B, black spectrum) revealed HFSs from ^{14}N and α-C-H (a_N = 2.05 mT, 3a_H = 2.76 mT), which are in agreement with previously

reported data for similar alkyl amine radical cations (*26*). The value of a_N close to 2.0 mT suggests a planar geometry at the nitrogen atom in this radical cation (*27*).

It is important to note that the experimental TREPR spectra of **R1•** generated with photocatalysts **PC1** (Fig. 2B, red spectrum) and **PC2** (Fig. 2B, blue spectrum) exhibited significant extent of hyperpolarization due to the chemically-induced dynamic electron polarization (CIDEP) (*28*). Interestingly, the polarization center of the two spectra matched the spectral centers of the reduced form of photocatalysts (g = 1.9875 and 2.0034 for **PC1**$^{\bullet-}$ and **PC2**$^{\bullet-}$, respectively, see Fig. S8). This observation indicates that the radical cation **R1•** originates from the geminate radical pairs generated by excited state SET, providing direct evidence for the electron transfer step (Fig. 2C). Remarkably, the observed absorption/emission (A/E)-type polarization pattern in both cases (see Fig. S7 for detailed analysis) indicates that the photoinduced SET with both photocatalysts occurs through the formation of an initial singlet radical pair (^{1}RP) (*29*, *30*, *31*). Thus, the singlet excited states of both [Ir(dF-CF$_3$-ppy)$_2$(dtbbpy)]PF$_6$ and 4CzIPN had a significant contribution to their photoredox activity in this reaction, which is in line with a recent study on the photoinduced SET between 4CzIPN and azide anion (*22*). This observation offers explicit information for the state of excited photocatalyst involved in the SET process.

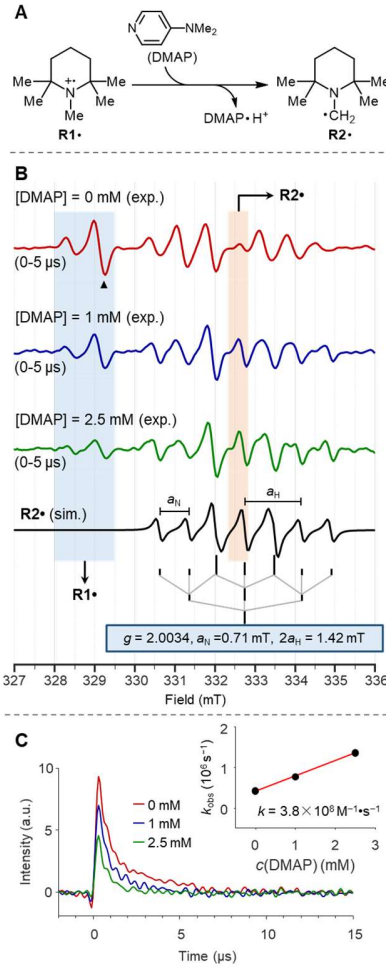

Fig. 3. Observing the formation of radical R2•. (**A**) The deprotonation reaction of **R1•**. (**B**) The TREPR spectra (0-5 μs integration after the laser pulse) with different DMAP concentrations. The peak marked with a black triangle was used to acquire the kinetic profiles. (**C**) Kinetic profiles of **R1•** with different DMAP concentrations.

Generation of α-aminoalkyl radical

Since the amine radical cation is believed to be a highly active intermediate, directly observing its transformation is of significant interest. With the help of the U-PSD EPR technique, we could elucidate the reactivity of the amine radical cation **R1•** through clear experimental evidence (Fig. 3A).

We performed the study on the reaction between PMP and **PC1** in the presence of different concentrations of DMAP as the base. Without an external base, **R1•** was found to be the major radical species observed in the TREPR spectrum (Fig. 3B, red spectrum). However, upon addition of DMAP, a new radical species started to appear while **R1•** was disappearing (Fig. 3B, blue spectrum). This new radical species was assigned as the α-aminoalkyl radical **R2•** based on its spectral characteristics. It was found that higher concentrations of DMAP resulted in a higher degree of conversion of **R1•** to **R2•** within the same time period (Fig. 3B, green spectrum). This observation indicates that the formation of **R2•** from **R1•** involves a deprotonation process, and DMAP is a more efficient base than PMP itself.

The spectral signature of **R2•** (Fig. 3B) indicates the HFS from both ^{14}N and α-C-H (a_N = 0.71 mT, 2a_H = −1.42 mT), which align with previously documented values of α-

aminoalkyl radicals (*32*). Compared with the coupling constant in the methyl radical ($3a_H = -2.30$ mT), the smaller amplitude from α-C-H of **R2•** suggests a pyramidalization of the α-aminoradical center (*27*), and the HFS of ^{14}N originates from spin delocalization.

For this deprotonation step, we not only observed the spectroscopic change but also acquired its kinetics by tracing the decay of **R1•** (Fig. 3C) and the formation of **R2•** (Fig. S9). As the concentration of base increased, the decay of **R1•** became faster, corresponding to the decrease in build-up intensity of the cation radical **R1•**. By fitting the kinetic traces of this series, the second-order rate constant for the proton transfer step was determined to be 3.8×10^8 $M^{-1}\cdot s^{-1}$ (Fig. 3C, inset, see Fig. S13 and Table S2 for details), accounting for the expected high reactivity of the amine radical cation. To the best of our knowledge, the transformation of amine radical cation to α-aminoalkyl radical has never been observed in such level of detail (*33*).

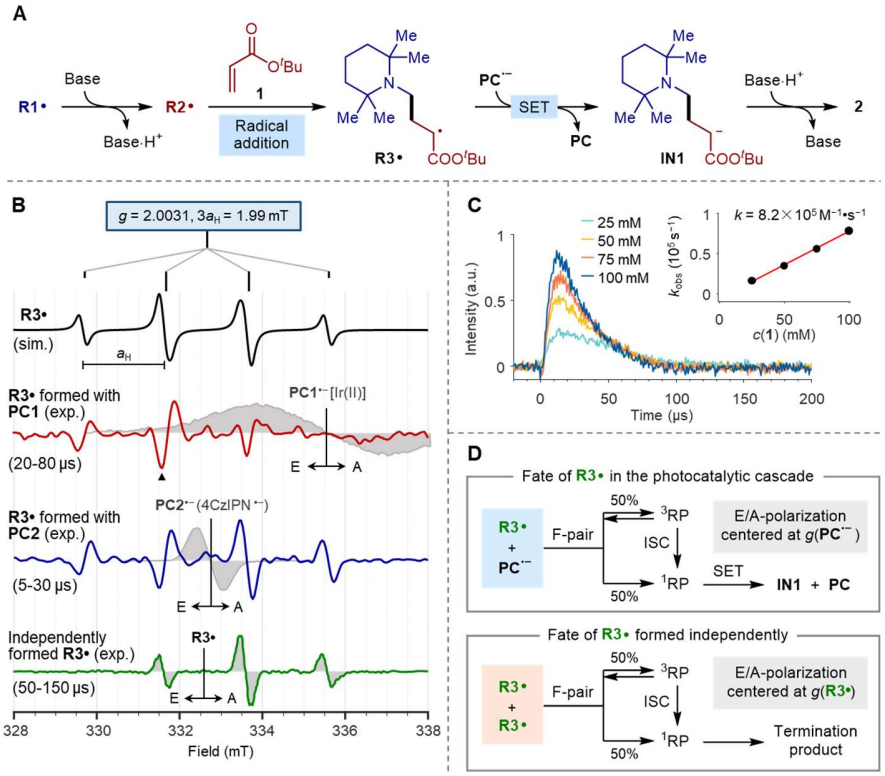

Fig. 4. Observing the radical addition and the subsequent SET reduction steps. (**A**) The reaction cascade from **R1•** to the final product. (**B**) The TREPR spectra of the radical **R3•**: Black (simulated steady-state spectrum), red (**R3•** generated with **PC1**), blue (**R3•** generated with **PC2**), green (independently generated **R3•** without a photocatalyst). The peak marked with a black triangle was monitored to acquire the kinetic profiles. (**C**) Kinetic profiles of **R3•** with different concentrations of *tert*-butyl acrylate. (**D**) Schematic interpretation of the polarization mechanism of **R3•**.

Radical addition and subsequent SET reduction

To further investigate the fate of the α-aminoalkyl radical **R2•** (Fig. 4A), we conducted TREPR measurements for the reaction system consisting of PMP, DMAP, acceptor **1**, and different photocatalysts. With both **PC1** and **PC2**, the same radical intermediate was observed in the carefully time-gated TREPR spectrum to observe the late-stage of the reaction (Fig. 4B, red and

blue spectra). In order to identify the nature of the observed radical, we performed an additional experiment involving the reaction between PMP, di-*tert*-butylperoxide (DTBP), and **1** to independently generate the radical intermediate under non-photocatalytic conditions (see Fig. S10 for details) (*34*). The acquired spectrum confirmed the formation of the identical radical intermediate, assigned as the radical adduct **R3•** (Fig. 4B, green spectrum). This radical exhibits degenerated hyperfine splitting from α- and β-C-H ($3a_H = -1.99$ mT), as revealed by the simulated steady-state EPR spectrum (Fig. 4B, gray, see Figs. S4, S11, S12 for details), which is in consistent with previously reported data for α-carbonyl radicals (*35,36*).

By monitoring the designated peak corresponding to the radical adduct **R3•** in the PMP/DMAP/**1**/**PC1** reaction system with varying concentrations of the acceptor **1**, we observed concentration-dependent changes in the kinetic profile of this radical intermediate (Fig. 4C). Non-linear fitting of the acquired kinetic data allowed us to obtain the second-order rate constant of 8.2×10^5 $M^{-1}\cdot s^{-1}$ for the radical addition (Fig. 4C, inset, see Fig. S14 and Table S3 for details), which is consistent with the magnitudes of the reported rate constants for the addition of α-aminoalkyl radicals to methyl acrylate (*34*).

The remaining puzzle of the whole photocatalytic cycle is the reaction pathway of **R3•**, specifically, how this radical transforms into the final product. It is believed that this step proceeds through an SET reduction/protonation process, supported by the redox potentials of **R3•** and $\mathbf{PC}^{\bullet-}$ (*37,38,39*). Additionally, another viable pathway involves hydrogen atom transfer (HAT) from the amine α-C-H bond, considering the bond dissociation energies (*40*,*41*). However, due to the lack of direct experimental evidence, the mechanism of this step remains an unanswered question.

Direct observation provided valuable mechanistic insights for this step. Looking into the TREPR spectra of **R3•** formed with **PC1** and **PC2**, we found that the observed E/A-type polarization fits the spectral centers of the reduced form of photocatalysts, Ir(II) and $4CzIPN^{\bullet-}$, respectively (Fig. 4B, red and blue spectra). This is in line with a characteristic free radical pair (F-pair) CIDEP mechanism (Fig. 4D, up), disclosing the interaction between **R3•** and $\mathbf{PC}^{\bullet-}$ (*30*). This clearly supported the SET reduction pathway in the present reaction. By comparison, we found that independently formed **R3•** in the absence of reduced photocatalyst exhibited E/A-type polarization with a different center (Fig. 4B, green spectrum), which fits into a scenario of F-pair CIDEP caused by self-termination of **R3•** (Fig. 4D, down) (*30*). The polarization pattern of the TREPR spectra served as an important probe for elucidating the mechanism of the SET process.

Summary

The present study demonstrates the U-PSD EPR technique as a powerful tool for elucidating the mechanistic complexity of radical transformations. It enables direct observation of radical cascade reactions, providing fine structure, kinetics, and spin dynamics of each radical intermediate, which makes visualization of a molecular photocatalytic cycle possible. The comprehensive mechanistic understanding gained by direct observation can aid in the rational design of more efficient photocatalytic systems. We believe that this research has the potential to make a significant impact in the field of radical research.

References and Note

1. Q. Wang, K. Domen, *Chem. Rev.* **120**, 919–985 (2020).
2. W. Zhang, A. R. Mohamed, W.-J. Ong, *Angew. Chem. Int. Ed.* **59**, 22894–22915 (2020).
3. L. Marzo, S. K. Pagire, O. Reiser, B. König, *Angew. Chem. Int. Ed.* **57**, 10034–10072 (2018).

4. J. M. R. Narayanam, C. R. J. Stephenson, *Chem. Soc. Rev*. **40**, 102–113 (2010).
5. Q. M. Kainz et al., *Science*. **351**, 681–684 (2016).
6. I. Ghosh, T. Ghosh, J. I. Bardagi, B. König, *Science*. **346**, 725–728 (2014).
7. H. Huo et al., *Nature*. **515**, 100–103 (2014).
8. D. A. Nagib, D. W. C. MacMillan, *Nature*. **480**, 224–228 (2011).
9. N. A. Romero, D. A. Nicewicz, *Chem. Rev.* **116**, 10075–10166 (2016).
10. C. K. Prier, D. A. Rankic, D. W. C. MacMillan, *Chem. Rev.* **113**, 5322–5363 (2013).
11. L. Buzzetti, G. E. M. Crisenza, P. Melchiorre, *Angew. Chem. Int. Ed.* **58**, 3730–3747 (2019).
12. K. Ishii, Y. Hirose, H. Fujitsuka, O. Ito, N. Kobayashi, *J. Am. Chem. Soc*. **123**, 702–708 (2001).
13. J. M. Ahn, T. S. Ratani, K. I. Hannoun, G. C. Fu, J. C. Peters, *J. Am. Chem. Soc.* **139**, 12716–12723 (2017).
14. R. Sreekanth, K. P. Prasanthkumar, M. M. Sunil Paul, U. K. Aravind, C. T. Aravindakumar, *J. Phys. Chem. A.* **117**, 11261–11270 (2013).
15. Y. Qin, R. Sun, N. P. Gianoulis, D. G. Nocera, *J. Am. Chem. Soc.* **143**, 2005–2015 (2021).
16. M. T. Colvin et al., *J. Am. Chem. Soc*. **133**, 1240–1243 (2011).
17. M. D. E. Forbes, L. E. Jarocha, S. Sim, V. F. Tarasov, in *Advances in Physical Organic Chemistry*, I. H. Williams, N. H. Williams, Eds. (Academic Press, 2013), vol. 47, pp. 1–83.
18. N. J. Turro, M. H. Kleinman, E. Karatekin, *Angew. Chem. Int. Ed.* **39**, 4436–4461 (2000).
19. L. Lewis-Borrell et al., *J. Am. Chem. Soc*. **143**, 17191–17199 (2021).
20. A. Bhattacherjee et al., *Nat. Commun*. **10**, 5152 (2019).
21. S. J. Greaves et al., *Science*. **331**, 1423–1426 (2011).
22. M. Sneha et al., *ACS Catal*. **13**, 8004–8013 (2023).
23. C. Karunakaran, M. Balamurugan, in *Spin Resonance Spectroscopy*, C. Karunakaran, Ed. (Elsevier, 2018), pp. 229–280.
24. S. Zhang, S. Zhou, J. Qi, L. Jiao, X. Guo, *Rev. Sci. Instrum.* **94**, 084101 (2023).
25. K. Nakajima, Y. Miyake, Y. Nishibayashi, *Acc. Chem. Res.* **49**, 1946–1956 (2016).
26. R. W. Fessenden, P. Neta, Mellon Inst. Sci., *J. Phys. Chem.* **76**, 2857–2859 (1972).
27. F. Gerson, W. Huber, *Electron Spin Resonance Spectroscopy of Organic Radicals* (John Wiley & Sons, 2003).
28. R. W. Fessenden, R. H. Schuler, *J. Chem. Phys.* **39**, 2147–2195 (1963).
29. L. J. Berliner, E. Bagryanskaya, in *Multifrequency Electron Paramagnetic Resonance* (John Wiley & Sons, Ltd, 2011), pp. 947–992.
30. M. D. E. Forbes, *Photochem. Photobiol.* **65**, 73–81 (1997).
31. J. Eills et al., *Chem. Rev*. **123**, 1417–1551 (2023).
32. D. E. Wood, R. V. Lloyd, *J. Chem. Phys*. **53**, 3932–3942 (2003).
33. S. Das, C. von Sonntag, *Z. Naturforsch. B*. **41**, 505–513 (1986).
34. J. Lalevée, B. Graff, X. Allonas, J. P. Fouassier, *J. Phys. Chem. A*. **111**, 6991–6998 (2007).
35. T. Foster, D. Klapstein, P. R. *West, Can. J. Chem.* **52**, 524–526 (1974).
36. B. Kubiak, M. Lehnig, W. P. Neumann, U. Pentling, A. K. Zarkadis, *J. Chem. Soc., Perkin trans.*, **2**, 1443–1447 (1992).
37. M. Schmittel et al., *Tetrahedron*. **65**, 10842–10855 (2009).
38. S. Ladouceur, D. Fortin, E. Zysman-Colman, *Inorg. Chem.* **50**, 11514–11526 (2011).
39. K. N. Swanick, S. Ladouceur, E. Zysman-Colman, Z. Ding, *RSC Advances.* **3**, 19961–19964 (2013).
40. L. J. J. Laarhoven, P. Mulder, D. D. M. Wayner, *Acc. Chem. Res.* **32**, 342–349 (1999).
41. J. M. Karty, G. A. Janaway, J. I. Brauman, *J. Am. Chem. Soc.* **124**, 5213–5221 (2002).

Acknowledgments:

The authors thank Prof. H. Mayr for proofreading the manuscript and Prof. M.-T. Zhang for helpful discussions.

Funding: This work was supported by Tsinghua University Dushi Program. The National Natural Science Foundation of China (Grant No. 22193011) is acknowledged for financial support.

Author contributions: X.G. and L.J. conceived the study. W.S. and J.-Q.Q. carried out the TREPR experiments. J.L. and S.S. completed the synthetic experiments and the characterization of the compounds. J.-Q.Q. completed the TREPR data post-processing. L.J., X.G. and J.-Q.Q. wrote the manuscript.

Competing interests: The authors declare no competing financial interests.

Data and materials availability: All data are available in supplementary materials.

Supplementary Materials

Materials and Methods
Supplementary Text
Figs. S1 to S14
Tables S1 to S3
References (S1-S2)
TREPR Dataset